

INSERT CREATIVE NAME HERE

Author's name

Bachelorarbeit in Physik
angefertigt im Argelander-Institut für Astronomie

vorgelegt der
Mathematisch-Naturwissenschaftlichen Fakultät
der
Rheinischen Friedrich-Wilhelms-Universität
Bonn

MMM 2024

DRAFT

Ich versichere, dass ich diese Arbeit selbstständig verfasst und keine anderen als die angegebenen Quellen und Hilfsmittel benutzt sowie die Zitate kenntlich gemacht habe.

Bonn,
Datum
Unterschrift

1. Gutachter: Prof. Dr. John Smith
2. Gutachterin: Prof. Dr. Anne Jones

Acknowledgements

I would like to thank ...

You should probably use \chapter* for acknowledgements at the beginning of a thesis and \chapter for the end.

DRAFT

Contents

1	Introduction	1
2	Theoretical Background	2
2.1	Clusters and groups of galaxies	2
2.1.1	The Intracluster Medium (ICM)	2
2.1.2	Emission Processes within the ICM	2
2.1.3	The galaxy group NGC1550	3
2.2	eROSITA	3
2.3	Skybackground and contamination sources	3
3	Data Reduction	5
3.1	Raw photon images	5
3.2	Image filtering	5
3.3	PIB-Correction	6
3.4	N_{H} Absorption Correction	7
4	Data Analysis	8
4.1	Image Visual Inspection	8
4.2	Surface Brightness Analysis	8
4.2.1	Full Azimuthal Surface Brightness Analysis	8
A	Appendix	11
A.1	PIB Map	11
	Bibliography	12
	List of Figures	13
	List of Tables	14

CHAPTER 1

Introduction

Testing Kolokythas et al., 2020. new line

CHAPTER 2

Theoretical Background

2.1 Clusters and groups of galaxies

Throughout the Universe, galaxies are not distributed homogeneously but are instead aggregated into massive cosmic structures known as galaxy groups or galaxy clusters. Galaxy clusters – the largest relaxed structures in the Universe – typically have masses exceeding $M \gtrsim 3 \times 10^{14} M_{\odot}$, whereas galaxy groups have masses around $M \sim 3 \times 10^{13} M_{\odot}$ (Schneider, 2006). Advancements in X-ray astronomy have demonstrated that these structures are significant sources of X-ray radiation (Cavaliere, Gurkaynak, and Tucker, 1971). This emission is well understood to originate from a hot intergalactic gas known as the intracluster medium (ICM), which is characterized by temperatures in the range of 10^7 to 10^8 K and constitutes the primary baryonic component of galaxy clusters (Schneider, 2006).

2.1.1 The Intracluster Medium (ICM)

Within the deep gravitational wells of galaxy clusters, the temperatures become sufficiently high to fully ionize lighter elements and partially ionize heavier elements, resulting in the formation of a plasma. This hot, diffuse, and optically thin plasma, known as the Intracluster Medium (ICM), emits significant amounts of X-ray radiation. X-ray analysis of the ICM have enabled a wide variety of cosmological studies, including large-scale structure formation in the Universe (Kravtsov and Borgani, 2012).

2.1.2 Emission Processes within the ICM

A key principle of electrodynamics is that accelerated charges radiate energy. This radiation is referred to as bremsstrahlung or "free-free" when a free charged particle, typically an electron, is accelerated by the electric field of other charges, usually ions. In the ICM, this process predominates at temperatures above $k_B T_e \gtrsim 2 \text{ keV}$, where the total emissivity at solar metallicity scales approximately as

$$\epsilon_{\text{ff}} \propto T_e^{\frac{1}{2}} n_e,$$

with n_e and T_e as the electron number density and temperature, respectively. At lower temperatures ($k_B T \lesssim 2 \text{ keV}$), line emission becomes significant, with the emissivity being roughly described by

$$\epsilon \propto T_e^{-0.6} n_e.$$

2.1.3 The galaxy group NGC1550

Insert cool stuff about cluster here

2.2 eROSITA

The extended ROentgen Survey with an Imaging Telescope Array (eROSITA) is a highly sensitive, wide-field X-ray telescope designed to capture deep and precise images across large areas of the sky. Mounted on the Spektrum-Roentgen-Gamma (SRG) observatory in a halo orbit around the second Lagrange Point, eROSITA operates within the 0.2 to 10.0 keV energy range. It is the first instrument to perform an all-sky imaging survey in the hard X-ray band (2.0 to 10.0 keV). In the soft X-ray band (0.5 to 2.0 keV), eROSITA boasts a sensitivity that is approximately 20 times greater than that of its predecessor, the ROSAT All-Sky Survey. eROSITA features seven identical mirror modules, known as Telescope Modules (TMs), each with 54 mirror shells in Wolter-I geometry and a 1.6-meter focal length. Five TMs (TM1, TM2, TM3, TM4, TM6) have aluminum on-chip optical light filters and are collectively referred to as TM8. The remaining two TMs (TM5, TM7), designed for low-energy spectroscopy, lack these filters and are referred to as TM9. (Predehl et al., 2021). Collectively, TM8 and TM9 are referred to as TM0.

2.3 Skybackground and contamination sources

For a thorough analysis of X-ray photons, it is essential to carefully consider both external background and internal instrumental contamination effects. The following section will provide a brief overview of the most important factors relevant to this analysis.

Cosmic X-ray Background (CXB): The Cosmic X-ray background comprises multiple sources, including diffuse, unabsorbed thermal emissions from the Local Hot Bubble, a plasma cavity surrounding the Sun, and absorbed thermal emissions from the Galactic halo (Galeazzi et al., 2006). Additionally, it includes discrete extragalactic sources, predominantly unresolved AGNs (Brandt and Hasinger, 2005). The diffuse component is more prominent in the lower energy band $\sim 1 \text{ keV}$, while the extragalactic sources dominate at higher energies.

Non-X-ray Background (NXB): The non-X-ray background consists of two main components: highly variable soft protons flares from the solar corona and Earth's magnetosphere, which can be focused onto detectors, and energetic Galactic Cosmic Ray (GCR) primaries, which interact with the detector to produce secondary particles. While primary GCR events can be mostly discarded by

onboard processing, the secondary particles deposit charge in the detector, making it challenging to distinguish them from true X-ray events. (Bulbul et al., 2020)

eROSITA light leak: Shortly after the launch of eROSITA, it was observed that CCDs lacking an on-chip filter (TM9) recorded a notably higher number of events. This was attributed to optical and ultraviolet light from the Sun entering the CCD through an unidentified gap in the detector shielding and was subsequently termed “light-leak” (Predehl et al., 2021).

N_{H} absorption: As X-rays travel to the detector, they undergo photoelectric absorption in the interstellar and intergalactic medium. The cross-section $\sigma \propto E^{-3.5}$ is inversely proportional to energy, causing a bias toward harder X-rays, as they interact less. Additionally, $\sigma \propto Z^5$ making metal abundance crucial for energies $\gtrsim 0.2 \text{ keV}$.

Table 2.1: Fit Parameters

Region	1	2	3	4
West	(2.38×10^{-5})	(5.47×10^{-1})	(1.11×10^2)	(1.01×10^{-7})
East	(2.31×10^{-5})	(4.96×10^{-1})	(9.2×10^1)	(1.05×10^{-7})
North	(1.69×10^{-5})	(4.53×10^{-1})	(8.1×10^1)	(8.08×10^{-8})
South	(4.72×10^{-5})	(4.99×10^{-1})	(6.67×10^1)	(9.53×10^{-8})

CHAPTER 3

Data Reduction

In the following section, the underlying data shall be reduced and corrected for the various effects and contamination sources explained in Section 2.3. Data from eRASSX is utilized for all TMs (1-7) using *eROSITA* pipeline processing version c010. The galaxy group NGC1550 is located in skytile 065087. In addition, the surrounding skytiles 062084, 062087, 062090, 065084, 065090, 068084, 068087, 068090 are used to encompass regions up to $\sim 3R_{200}$. The data reduction is performed with the software HEASoft version XXX and the extended Science Analysis Software System (eSASS 4DR1). Images were created using astropy.

3.1 Raw photon images

Before the data reduction process, raw photon images for all combined skytiles and TMs are presented across the following energy bands: 0.2 to 2.3 keV, 2.3 to 6.0 keV, and 6.0 to 9.0 keV. The skytiles were combined using the *eSASS* task `evtool`, with no additional parameters applied to reveal all inherent deficiencies in the raw images. The raw photon images are presented in 3.1. As observed, most cluster emission is concentrated in the lower energy band, making it the focus for detecting emission structures. In this analysis, the 0.2 to 2.3 keV energy band is used. Due to the light-leak in TM9, however, the energy range is restricted to 0.8 to 2.3 keV, while for TM8 it remains 0.2 to 2.3 keV. Hereafter, this TM-dependent energy band will be referred to as the “soft band” and the 6.0 to 9.0 keV energy range as the “hard band”.

3.2 Image filtering

Each skytile is cleaned individually using `evtool` with `pattern=15` to select all event patterns and `flag=0xc00fff30` to remove bad pixels and CCD corners. Subsequently, soft proton flares are identified and mitigated through the following process: the `flaregti` task is used to generate light curves with 20 s time bins in the energy range of 5 to 10 keV. A 3σ threshold is determined; time intervals exceeding this threshold indicate elevated count rates likely due to soft proton flares. The task `flaregti` is then rerun using this threshold to establish good-time-intervals (GTIs) excluding these

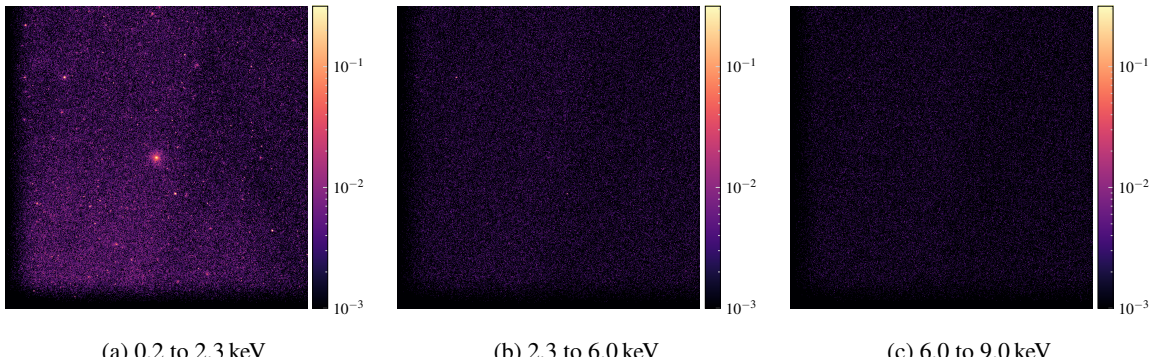


Figure 3.1: Raw photon images from TM0 of all combined skytiles centered around NGC1550, displayed in the energy bands 0.2 to 2.3 keV, 2.3 to 6.0 keV, and 6.0 to 9.0 keV, with Gaussian smoothing of 4 pixels applied. The colorbar represents (smoothed) photon counts. Most of the cluster emission is visible in the lower energy band (0.2 to 2.3 keV). A noticeable count drop on the right side of the images is evident and will be addressed through the exposure map correction detailed in Section X.

flare periods, which are applied using `evtool` with the `gti="FLAREGTI"` parameter. All SPF-filtered and cleaned skytiles are combined into a single TM0 photon image using `evtool`. Hereafter, these combined images shall be referred to as “filtered”. The `evtool` task with the `telid` parameter is also used to split the filtered photon images into individual filtered images for each TM, as needed for subsequent steps.

3.3 PIB-Correction

Subtracting the particle-induced background (PIB) from the combined filtered photon image is necessary. The following approach is based on extensive studies of the *e*ROSITA FWC data conducted by Dr. F. Pacaud, as utilized for example in Reiprich et al., 2021. The PIB is modeled for each TM using filter wheel closed (FWC) data. Due to the minimal spatial variation of the PIB, this modeling utilizes the flat exposure map created with the *e*SASS task `expmap`. Furthermore, given the negligible spectral variation, the counts H_{obs} in the hard band, where PIB counts dominate, is used to estimate the PIB contribution in the soft bands by multiplication with the ratio R of the number of FWC counts in the soft band S_{FWC} to the hard band H_{FWC} . A background map for each TM is then generated by applying this factor to the flat exposure map, normalized to 1 by dividing by the sum of all pixel values (norm. exposure map). Hence, the PIB map of a given TM is given by

$$\text{PIB map}_{\text{TM}} = H_{\text{obs}} R \cdot (\text{norm. exposure map})$$

PIB corrected image are obtained by subtracting the PIB map of each TM from the respective filtered photon image. The complete image for TM0 is obtain by co-adding all PIB corrected images. Furthermore, individual background maps are also co-added to form a complete PIB map, which can be found in Appendix A.1. Figure 3.2 compares the TM0 filtered image before and after PIB correction.

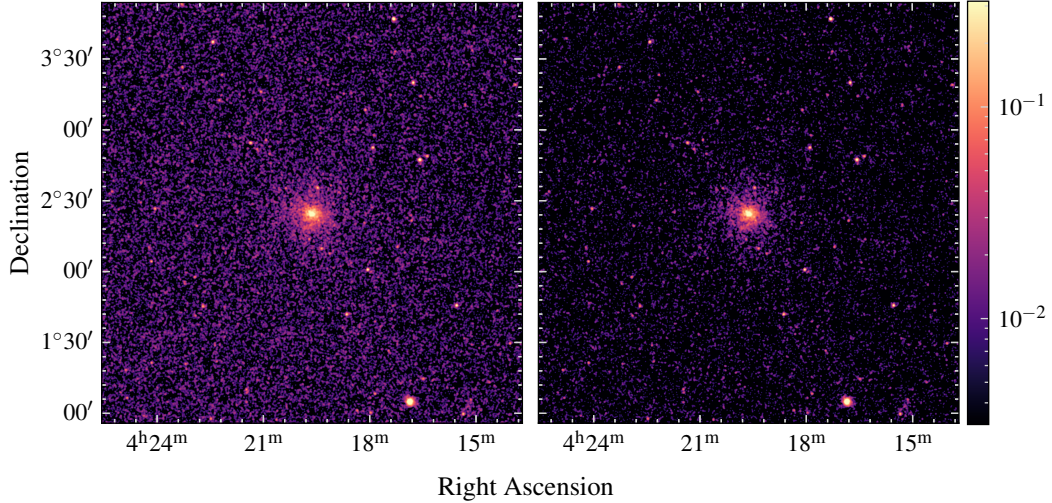


Figure 3.2: Photon images of NGC1550 in the soft band with Gaussian smoothing of 4 pixels. Left: SPF-filtered and cleaned image. Right: image after PIB correction. The colorbar represents smoothed counts, same scaling is used for comparison.

3.4 N_{H} Absorption Correction

As discussed in Section 2.3, X-ray absorption by the ISM must be considered. At higher energies ($\gtrsim 0.28 \text{ keV}$), as is relevant for this analysis, metals from stellar processes play a significant role. Assuming solar metallicity, the hydrogen column density along the line of sight can serve as an indicator of the amount of absorbing material. This involves utilizing the total hydrogen column density, including all its states neutral, molecular, or ionized. A cutout of the HI4PI all sky survey is therefore reprojected on to the relevant skytiles.

Data Analysis

4.1 Image Visual Inspection

4.2 Surface Brightness Analysis

4.2.1 Full Azimuthal Surface Brightness Analysis

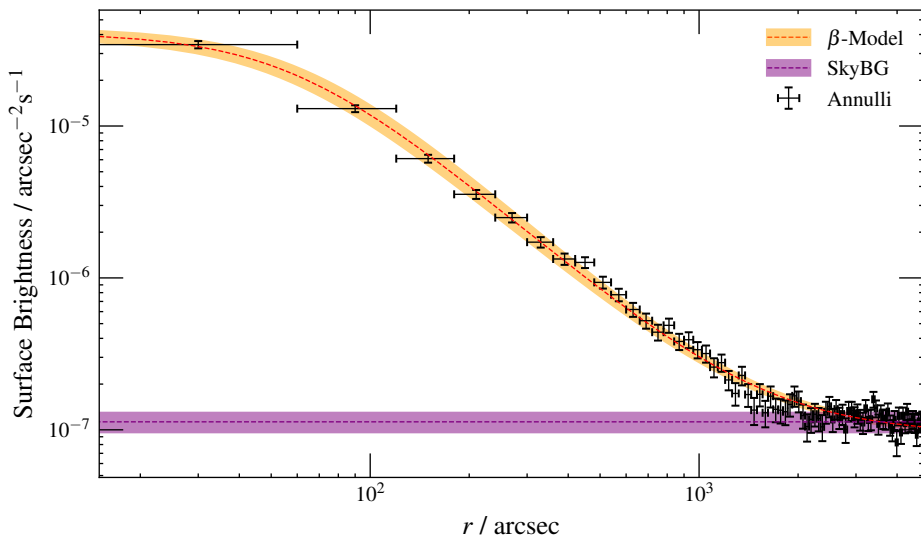


Figure 4.1: A nice plot.

To accurately quantify potential asymmetries in the X-ray emission of NGC 1550, a surface brightness analysis is performed. First, the emission center is estimated by constructing a 2' aperture around the apparent center, as given in Section X. This aperture size is chosen to capture a statistically significant number of photons while minimizing bias from potential asymmetries outside the group

center. The flux-weighted average of the image coordinates within this aperture yields a right ascension of 64.909° and a declination of 2.414° . Concentric Annulli with $1'$ width are constructed from the calculated flux-weighted surface brightness of the group up to $80'$. The counts C within each annulus are determined using the `funcnts` task from the `funtools` software, with a Poisson error of \sqrt{C} . The surface brightness S for each annulus is calculated by

$$S = \frac{C_{\text{image}} - C_{\text{PIB}}}{C_{\text{expmap}} \cdot A},$$

where C denotes the counts in the photon image, total PIB map, and exposure map, respectively. Errors are calculated using Gaussian error propagation. Furthermore, background estimation is performed using 10 circular regions with a $48'$ radius, each centered $160'$ from the calculated center of NGC 1550. The average background surface brightness is evaluated for all circles combined and separately for the northern (Circles 1-5) and southern regions (Circles 6-10) to account for possible background gradients.

Appendix

APPENDIX A

Appendix

A.1 PIB Map

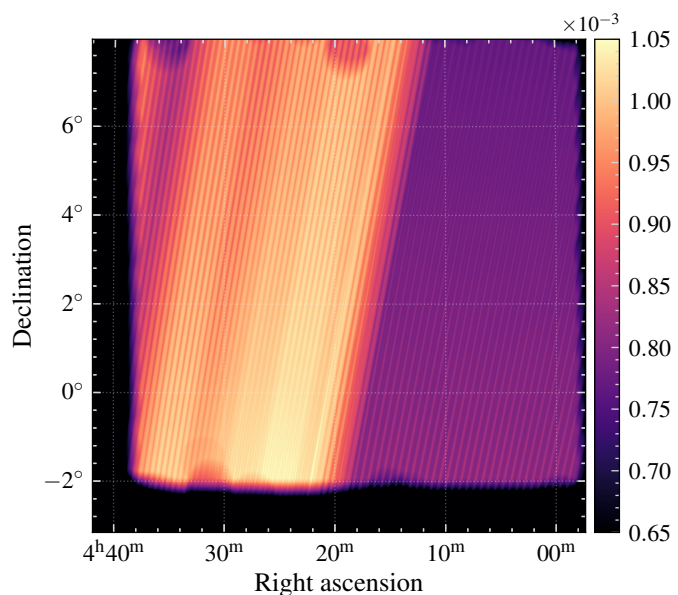


Figure A.1: PIB map created by co-adding individual background maps for each telescope module (TM).

Bibliography

- Brandt, W. and G. Hasinger (2005), *Deep Extragalactic X-ray Surveys*, Annual Review of Astronomy and Astrophysics **43** 827, First published online as a Review in Advance on June 14, 2005 (cit. on p. 3).
- Bulbul, E. et al. (2020), *Characterization of the Particle-induced Background of XMM-Newton EPIC-pn: Short- and Long-term Variability*, The Astrophysical Journal **891** 13, URL: <https://dx.doi.org/10.3847/1538-4357/ab698a> (cit. on p. 4).
- Cavaliere, A. G., H. Gurksy, and W. H. Tucker (1971), *Extragalactic X-ray Sources and Associations of Galaxies*, Nature **231** 437, ISSN: 1476-4687, URL: <https://doi.org/10.1038/231437a0> (cit. on p. 2).
- Galeazzi, M., A. Gupta, K. Covey, and E. Ursino (2006), *XMM-Newton observations of the diffuse X-ray background*, Department of Physics, University of Miami (cit. on p. 3).
- Kolokythas, K. et al. (2020), *Evidence of AGN feedback and sloshing in the X-ray luminous NGC 1550 galaxy group*, Monthly Notices of the Royal Astronomical Society **496** 1471, ISSN: 1365-2966, URL: <http://dx.doi.org/10.1093/mnras/staa1506> (cit. on p. 1).
- Kravtsov, A. V. and S. Borgani (2012), *Formation of Galaxy Clusters*, Annual Review of Astronomy and Astrophysics **50** 353, ISSN: 0066-4146, eprint: <https://www.annualreviews.org/doi/pdf/10.1146/annurev-astro-081811-125502>, URL: <https://www.annualreviews.org/doi/10.1146/annurev-astro-081811-125502> (cit. on p. 2).
- Predehl, P. et al. (2021), *First science highlights from SRG/eROSITA: The eROSITA X-ray telescope on SRG*, A&A **647** A1 (cit. on pp. 3, 4).
- Reiprich, T. H. et al. (2021), *The Abell 3391/95 galaxy cluster system: A 15 Mpc intergalactic medium emission filament, a warm gas bridge, infalling matter clumps, and (re-) accelerated plasma discovered by combining SRG/eROSITA data with ASKAP/EMU and DECam data*, AandA **647** A2, URL: <https://doi.org/10.1051/0004-6361/202039590> (cit. on p. 6).
- Schneider, P. (2006), *Extragalactic Astronomy and Cosmology: An Introduction*, Second Edition, Springer-Verlag Berlin Heidelberg 2006, ISBN: 978-3-642-54082-0 (cit. on p. 2).

List of Figures

3.1	Raw photon images from TM0 of all combined skytiles centered around NGC1550, displayed in the energy bands 0.2 to 2.3 keV, 2.3 to 6.0 keV, and 6.0 to 9.0 keV, with Gaussian smoothing of 4 pixels applied. The colorbar represents (smoothed) photon counts. Most of the cluster emission is visible in the lower energy band (0.2 to 2.3 keV). A noticeable count drop on the right side of the images is evident and will be addressed through the exposure map correction detailed in Section X.	6
3.2	Photon images of NGC1550 in the soft band with Gaussian smoothing of 4 pixels. Left: SPF-filtered and cleaned image. Right: image after PIB correction. The colorbar represents smoothed counts, same scaling is used for comparison.	7
4.1	A nice plot.	8
A.1	PIB map created by co-adding individual background maps for each telescope module (TM).	11

List of Tables

2.1 Fit Parameters	4
------------------------------	---